

UNCLASSIFIED

AD 91939

Armed Services Technical Information Agency

Reproduced by

DOCUMENT SERVICE CENTER

KNOTT BUILDING, DAYTON, 2, OHIO

This document is the property of the United States Government. It is furnished for the duration of the contract and shall be returned when no longer required, or upon recall by ASTIA to the following address: Armed Services Technical Information Agency, Document Service Center, Knott Building, Dayton 2, Ohio.

NOTICE: WHEN GOVERNMENT OR OTHER DRAWINGS, SPECIFICATIONS OR OTHER DATA ARE USED FOR ANY PURPOSE OTHER THAN IN CONNECTION WITH A DEFINITELY RELATED GOVERNMENT PROCUREMENT OPERATION, THE U. S. GOVERNMENT THEREBY INCURS NO RESPONSIBILITY, NOR ANY OBLIGATION WHATSOEVER; AND THE FACT THAT THE GOVERNMENT MAY HAVE FORMULATED, FURNISHED, OR IN ANY WAY SUPPLIED THE SAID DRAWINGS, SPECIFICATIONS, OR OTHER DATA IS NOT TO BE REGARDED BY IMPLICATION OR OTHERWISE AS IN ANY MANNER LICENSING THE HOLDER OR ANY OTHER PERSON OR CORPORATION, OR CONVEYING ANY RIGHTS OR PERMISSION TO MANUFACTURE, USE OR SELL ANY PATENTED INVENTION THAT MAY IN ANY WAY BE RELATED THERETO.

UNCLASSIFIED

**Best
Available
Copy**

FC

**NEVIS CYCLOTRON
LABORATORIES**

**COLUMBIA UNIVERSITY
PHYSICS DEPARTMENT
Irvington-on-Hudson,
New York**

**Joint ONR - AEC Program
Office of Naval Research Contract
Contract N6-ori-110 Task No. 1**

**AD No. 711
ASTIA FILE COPY**

Nevis - 14
R - 110
CU - 90

Nevis Cyclotron Laboratories
Columbia University
Department of Physics
Irvington-on-Hudson,
New York

78 Mev π^{\pm} SCATTERING FROM LITHIUM

Ross Williams, James Rainwater and
Aihud Pevsner

CU-90-55-ONR-110-1-Physics

Submitted in partial fulfillment
of the requirements for the degree
of Doctor of Philosophy in the
Faculty of Pure Science, Columbia
University

August, 1955

Joint ONR-AEC Program
Office of Naval Research Contract
Contract N6-ori-110-Task No.1

78 Mev π^{\pm} Scattering from Lithium*

Ross Williams,** James Rainwater, and Aihud Pevsner***
Columbia University, New York, New York

August, 1955

-
- * This research was supported by the Joint Program of the Office of Naval Research and the Atomic Energy Commission.
- ** Now at Paul Rosenberg Associates, Mount Vernon, New York,
- *** Now at Massachusetts Institute of Technology, Cambridge, Massachusetts.
-

ABSTRACT

The angular distributions of 78 Mev π^{\pm} scattered elastically from lithium have been measured. The distributions have been analyzed by combining coherently the scattering amplitudes for the individual pion-nucleon interactions, and weighting each amplitude by a form factor determining the ability of the struck nucleon to absorb the momentum recoil and remain in its same state in a nuclear harmonic oscillator well. Corrections are applied for solid angle transformations between the pion-nucleus and pion-nucleon center of mass systems, the effect of the required nuclear elastic scattering upon the available phase space in the pion-nucleon system, and an initial momentum distribution for the nucleons. The simple Born approximation treatment provides agreement with the pronounced dip at 75° and the backward rise of the experimental curves.

A. INTRODUCTION

An examination of the "elastic"* scattering of (78 ± 4.7) Mev positive and negative pions from lithium has been made. This represents an extension of previous measurements of the scattering on aluminum as part of our program of investigating the behavior of the angular distribution of the elastic scattering of pions on complex nuclei. The variable parameters, in addition to the angle, are the pion charge and energy, and the atomic number of the target nucleus.

* The sum of true elastic plus nearly elastic scattering is actually measured. The term "elastic" for the experimental results will usually imply this sum.

The familiar optical model method,¹ generalized here to

¹ Fernbach, Serber, and Taylor, Phys. Rev. 75, 1352 (1949)
K. M. Watson, Phys. Rev. 89, 575 (1953)

treat the scattering from a nucleus as a solution to a Schrodinger equation involving a central potential, has been applied to the scattering of fast nucleons by nuclei with relatively good agreement with experiment.²

² R. D. Woods and D. S. Saxson, Phys. Rev. 95, 577 (1954)
F. Rohrlich and D. M. Chase, Phys. Rev. 94, 81 (1954)
B. I. Cohen and R. V. Neidigh, Phys. Rev. 93, 282 (1954)
P. C. Gugelot, Phys. Rev. 87, 525 (1952)

R. E. Le Levier and D. S. Saxon, Phys. Rev. 87, 40 (1952)

J. W. Burkig and B. T. Wright, Phys. Rev. 82, 451 (1951)

Optical model solutions³ have also been obtained for positive

³ A. Pevsner and J. Rainwater, to be published.

and negative pions incident upon an aluminum nucleus, whose potential is represented by the coulomb potential beyond the nuclear radius and a complex square well (with various choices of complex potential) within the nuclear radius.

The usual optical model does not make use of the angular distribution of the elementary pion-nucleon scattering process, but uses only the forward scattering amplitude $f(0)$. Thus the predicted angular distribution of the scattering is determined by the nuclear density distribution and the forward scattering amplitude $f(0)$ for neutrons and protons. An opposite extreme approach can be based on the Born approximation or "impulse approximation" (linear superposition) which uses the complete angular dependence of the elementary pion-nucleon scattering amplitudes $f(0)$, modified by a form factor due to nuclear size. Since the elementary $f(0)$ are quite asymmetric, with strong minima near 90° , the two methods lead to rather different predictions for the expected angular distribution. (Recently a modified optical analysis has been developed which should take better account of $f(0)$.⁴) The experimental results for pion

⁴ L. S. Kisslinger, Phys. Rev. 98, 761 (1955)

scattering by lithium showed an angular dependence of the type that one would expect from the Born approximation analysis, and we have used this analysis for comparison with experiment.

B. EXPERIMENTAL ARRANGEMENT

The experimental conditions are substantially the same as those reported for measuring the angular distribution from aluminum.⁵ In brief summary, mesons with a continuous spread

⁵ Pevsner, Rainwater, Williams and Lindenbaum, to be published.

of momenta are produced when circulating protons strike a beryllium target near the exit window of the Nevis 385 Mev cyclotron. Mesons of approximately 170 Mev/c momentum are able to escape through one of the narrow channels in the cyclotron shielding wall to produce a roughly monoenergetic 80 Mev meson beam in the experimental area. Figure 1 shows the floor plan of the experiment. A focussing magnet at the exit of the wall channel acts as a more refined momentum selector, and through its focussing action intensifies the meson beam in the direction of the incident telescope (crystals 1 and 2, Figure 1).

A plastic scintillator 4" x 2" x 1/4" was used in the first counter, C1. The second counter, C2, contained a 3" x 3/4" x 3/16" stilbene crystal and was placed approximately 40" behind the first, where it served to define the direction and lateral extent of the beam incident upon the lithium target. The target itself was a 14" x 7" x 2" piece of pure lithium wrapped

in very thin nylon for air and moisture protection. The lithium could be rotated in a vertical plane about the two mounting pivot points directly behind crystal 2. Although the lithium was large in lateral extent, its effective lateral dimensions were determined by those of crystal 2 placed directly in front of it. Those mesons which were scattered by the lithium could be counted by counters 3 and 4, spaced 4" apart and as far from the lithium target as the compromise between good angular resolution and reasonable counting rates would allow. Angular resolution actually varied from $\pm 1.9^\circ$ near the forward direction to $\pm 4.8^\circ$ near the minimum of the curve. Counters C3 and C4 contained stilbene crystals 4" x 2" x 1/8" and 4" x 2" x 1/4" respectively. 3/4" copper was placed between counters 3 and 4 to prevent all but the elastically* scattered mesons from registering in counter 4. To obtain an angular distribution, counters 3 and 4 were rigidly mounted upon two aluminum rods which could be rotated through 360° in a vertical plane about the two pivot points holding the lithium target. The "long" dimension of all counters was made horizontal to permit the use of a relatively large beam area and detector telescope solid angle, while maintaining good angular resolution.

The outputs from the photomultipliers were amplified, using broad-band amplifiers, and then sent to bridge and 6BN6 type fast (10^{-8} sec.) coincidence circuits in the following pairs: C1 and C2, C1 and C3, C2 and C4. From the coincidence circuits pulses were sent through cathode followers and 300' of cable to discriminators and pulse shapers in the laboratory building. The pulses were then applied to a relatively slow (10^{-7} sec.) Rossi-type triple coincidence circuit which provided an output pulse whenever the C1-C2, C1-C3, and C2-C4 counts appeared simul-

taneously. Such a pulse, resulting from a particle passing through all four counters, was sent to a scale of 64 circuit (5 μ sec. resolution).

C. EXPERIMENTAL MEASUREMENTS

The focussing magnet, acting as a momentum selector, produced a beam of 80.8 ± 4.0 Mev mesons in the C1-C2 telescope. The thickness of the lithium target caused an energy loss and further spread, such that the effective pion energy at scattering was 78.0 ± 4.7 Mev. To insure that only "elastically" scattered pions were measured, 3/4" of copper was placed between C3 and C4 whenever the lithium target was in position immediately behind C2. (A pion must have roughly 65 Mev kinetic energy to escape from the target and traverse 3/4"Cu.) When the target was removed for background runs, an additional 1/4" of copper was added to compensate for the lithium thickness. Before each set of runs, the incident beam was analyzed by aligning all four counters in the median plane, and recording the number of quadruple counts obtained for a given number of C1-C2 counts, while varying the thickness of copper between C3 and C4 from zero to 2-1/4". A typical range curve so obtained is shown in Figure 2. In addition to the pronounced break in the curve at 1-1/4" (corresponding to 80.8 Mev pions), a small μ meson peak is evident at 1-3/4". The presence of a small electron contamination is shown by the final tail of the curve. The initial slope is due to nuclear interactions in flight by the pions.

In the measurement of the angular distribution, we make

use of the difference in overall coincidence rate between $3/4$ " and $(1-1/2 - t_{L1})$ " of copper between C3 and C4, where t_{L1} is the average equivalent copper thickness for a particular scattering angle, of that part of the lithium target yet to be traversed at the time of scattering. Thus a scattered meson must penetrate an equivalent copper thickness $t_1 = (3/4 + t_{L1})$ ", but fail to penetrate $t_2 = 1-1/2$ " of copper to be considered in the overall count. The background rate can be subtracted out by repeating the difference method described above, this time with the target absent. The true counting rate is then (in terms of target location and copper thickness)

$$[(In, t_1) - (In, t_2)] - [(Out, t_1) - (Out, t_2)].$$

In practice it was found that the counting rates (In, t_2) and (Out, t_2) were essentially the same, and therefore at most angles these two measurements were not made. The expression above then reduces to the target in minus target out rate at thickness $t_1 = (3/4 + t_{L1})$ " of absorber, and this is the manner in which the majority of the runs were actually made.

A number of necessary corrections to the C1-C2 monitoring counting rate can be made simultaneously by noting that the change in the forward beam range curve rate between thicknesses t_1 and t_2 of copper, divided by the rate for no absorber, gives the fraction of the incident beam which is effective for elastic scattering measurements (provided further correction is made for the 90 percent counting efficiency described below). Since the change in the range curve in going from t_1 to t_2 is almost entirely due to pions of the proper energy for "elastic"

scattering, this procedure automatically corrects for incident beam contamination, pions scattered in the sample with appreciable energy loss (inelastic), and for pion interactions in flight in the copper absorber. Hence multiplying the recorded C1-C2 rate by the fraction described above provides a corrected value of the incident flux for use in the cross-section computations. (At this point it should be noted that the scattering of muons and electrons is very small compared to that of the pions at angles larger than those for which multiple coulomb scattering predominates. Thus the C4-C3 scattered beam essentially contains only elastic or nearly elastic scattered pions, and no longer range particles.)

To measure the angular spread of the beam leaving the target the lithium target was positioned behind C2 and the angular distribution of quadruple counts shown in Figure 3 was obtained by swinging C3 and C4 through small angles about the forward direction. Called "beam spread", the angular distribution of Figure 3 actually included inherent spread in the incident beam, multiple coulomb scattering in the lithium, spread due to the angle subtended by the widths of C3 and C4, and π - μ decay between C2 and C4. From Figure 3 the full angular width at half maximum is approximately 4.0° . Since all of the causes of beam spread just cited are statistically independent of the large angle nuclear scattering, the beam spread curve can be looked upon as a resolution function operating on the nuclear single scattering to give the observed scattering. The fact that the beam spread curve was not greatly different with the lithium target in position and removed from the beam indicates

that multiple coulomb scattering was not the dominant cause of beam spread. Calculations of the expected multiple coulomb scattering agree with this result. Moving C3 and C4 closer to the target during actual runs to increase counting rates produced the angular resolutions listed in Table 1 for various angles.

To minimize and standardize energy loss of pions in the lithium target, the target was always set at one-half the angle of scattering. Scattering at angles less than 15° was not measured because of the large relative importance of multiple coulomb scattering, τ - μ decay of main beam pions, and undeflected main beam particles in this region.

Cross sections were calculated by subtracting the target-out from target-in quadruple counts for a given number of C1-C2 monitor counts, and then dividing by the C1-C2 counts, the number of effective nuclei per cm^2 in the target, and the solid angle subtended by C4 at the target. The C1-C2 rate was adjusted for beam contamination and counting efficiency as described above, and the effective thickness of the lithium target computed for each angle of scattering. Results are shown in Table 1 for 78 Mev π^- and π^+ . The \pm values listed are the statistical standard deviations.

D. INTERPRETATION OF RESULTS

Several features of the angular distributions listed in Table 1 and shown in Figures 4 and 5 suggest the importance of single nucleon scattering in the cross-section for lithium:

- a. The pronounced dip in the lithium cross section at 75° corresponds, after a transformation be-

tween the two center of mass systems, to the minimum in the single nucleon scattering near 90° .

- b. The cross section has the pronounced backward rise characteristic of the (π^+, p) or (π^-, n) interaction (assuming charge independence).
- c. At backward angles the π^- curve lies well above the π^+ curve. In this region and at 78 Mev, the (π^-, n) or (π^+, p) interaction (pure isotopic spin $3/2$ states) far outweighs that due to (π^-, p) or (π^+, n) . Neglecting the latter, the four neutrons and three protons of the lithium nucleus would favor a higher π^- than π^+ backward scattering by 4:3 for incoherent addition and 16:9 for coherent, apart from other corrections.
- d. The first four points for π^- and π^+ demonstrate the interference between nuclear and coulomb scattering below $\sim 30^\circ$. This interference, which was also observed for aluminum, is constructive for π^- and destructive for π^+ . The theoretical curves in Figures 4 and 5 do not include coulomb effects and help serve as reference curves to demonstrate the effect.

For a nucleus of spin 0, elastic scattering corresponds to coherent scattering leaving the state of the nucleus un-

changed. Li^7 has spin $3/2$, and thus there is a degeneracy effect corresponding to spin flip processes, even for strictly elastic scattering. In the subsequent discussions we neglect this effect and assume that only coherent scattering leaving the internal state of the nucleus undisturbed is of importance. For simplicity, and to give the effect of a diffuse nuclear surface, we use nucleon wave functions in a harmonic oscillator potential, with two protons and two neutrons in the ground state and one proton and two neutrons in the first excited state. The unnormalized nucleon wave functions can be written as

$$\psi_0 = e^{-\frac{(x^2 + y^2 + z^2)}{2}} \text{ for the ground state} \quad (1)$$

$$\psi_1 = \begin{pmatrix} x \\ y \\ z \end{pmatrix} e^{-\frac{(x^2 + y^2 + z^2)}{2}} \text{ for the first excited state} \quad (2)$$

where the unit length is taken as the s.h.o. length factor = $(\hbar/m\omega)^{1/2}$.

The interaction matrix element involves an integration over all nucleon coordinates as well as those of the meson. The latter integration leads to the pion-single nucleon scattering amplitude, whereas the former becomes a weighting factor whose magnitude is determined by the probability that all nucleons remain in their unperturbed states following the collision. Experimental conditions require that the meson scatter "elastically" from the nucleus as a whole in order to register a quadruple count. If it is assumed that the entire momentum transfer, as determined by the pion-nucleus elastic scattering, is given to a single nucleon, the weighting factor is given by a sudden perturbation or

a Born approximation treatment as

$$b_0 = \frac{\int \Psi_0^* e^{2iax} \Psi_0 d\tau}{\int |\Psi_0|^2 d\tau} = e^{-a^2} \quad \text{for the struck nucleon in the ground state and the } \left(\frac{y}{z}\right) e^{-\frac{r^2}{2}} \text{ excited states of the harmonic well,} \quad (3)$$

and

$$b_1 = \frac{\int \Psi_0^* e^{2iax} \Psi_1 d\tau}{\int |\Psi_1|^2 d\tau} = (1-2a^2)e^{-a^2} \quad \text{for the struck nucleon in the } xe^{-\frac{r^2}{2}} \text{ excited state.} \quad (4)$$

In equations (3) and (4), x is chosen as the direction of momentum transfer. Since Ψ_0 and Ψ_1 of equations 1, 2, 3 and 4, are in "natural" length units, the momentum transfer $2a$ must be evaluated in corresponding units. To this end the size of the harmonic well must first be established, and then the expectation value of the nucleon kinetic energy found. A reasonable criterion for well size can be had by requiring that $\langle r^2 \rangle$ for the nucleons be the same as for the more commonly used model which assumes constant density with a sharp edge at $R = r_0 A^{1/3}$. The resulting radius coefficient r_0 is chosen in accordance with other evidence:

$$\langle r^2 \rangle = (n + 3/2)_{AV} \frac{\hbar}{m\omega} = \left(\frac{3/2 \times 4 + 5/2 \times 3}{7} \right) \frac{\hbar}{m\omega} = 1.93 \frac{\hbar}{m\omega} = (3/5) r_0^2 A^{2/3} \quad (5)$$

We have chosen $r_0 = 1.28 \times 10^{-13}$ cm, $A = 7$ for lithium. The quantity in parentheses is a weighted average of $(n + 3/2)$ over the seven nucleons.

The expression (5) defines ω , and hence the harmonic well

size. The expectation value of kinetic energy in the x direction is:

$$1/3 \langle \text{K.E.} \rangle = 1/6 (n + 3/2) \hbar \omega = \frac{\hbar \omega}{4} \text{ for the ground state} \quad (6)$$

and

$$1/3 \langle \text{K.E.} \rangle_0 = \left\langle \frac{c^2 p^2}{2mc^2} \right\rangle_0 \quad (7)$$

giving

$$\langle c^2 p^2 \rangle_0 = (102.3 \text{ Mev})^2$$

In the same units,

$$\langle k^2 \rangle_0 = \frac{\int e^{-x^2/2} \frac{\partial^2}{\partial x^2} e^{-x^2/2} dx}{\int e^{-x^2} dx} = 1/2 \text{ for the ground state.} \quad (8)$$

$$\text{Hence } \langle k^2 \rangle = 1 \text{ corresponds to } \langle c^2 p^2 \rangle = (144.7 \text{ Mev})^2. \quad (9)$$

The unit of "natural" momentum is then 144.7 Mev.

The coordinates involved in equations 3 and 4 have origin at the center of mass of the nucleons as a whole, and the collision is treated as elastic with respect to the nucleus as a whole to establish overall conservation of energy and momentum. The entire momentum transfer is considered to be concentrated initially on the struck nucleon, so it receives a (non-relativistic) velocity change 7 times that of the nucleus center of mass. Thus the relative momentum change for the struck nucleon is reduced by the factor $(A-1)/A$ to give

$$2a = \frac{6/7 \Delta c p_{\pi}}{144.7 \text{ Mev}} \quad (10)$$

defining a of equations 3 and 4.

The value of λ used for the cross-section calculations is that of the meson in the pion nucleon center of mass system before collision. The fact that overall conservation of energy and momentum is relative to an elastic collision on the nucleus as a whole decreases the kinetic energy transfer to the struck Li nucleus compared to the amount that would be transferred to a free nucleon. (For 180° scattering a pion of 78 Mev initial kinetic energy has 69.9 Mev after being scattered elastically by Li and would have only 38.0 Mev after being scattered by a nucleon at rest.) Thus the (scalar) momentum of the pion in the pion-nucleon c.m. system is greater after scattering than before (scattering off the energy shell). This last effect complicates the calculation of the single nucleon scattering contributions.

All four nucleons in the ground state of the harmonic well are governed by the b_0 probability amplitude, as well as two-thirds of those in the first excited state (those for which $\Psi_1 \sim \begin{pmatrix} y \\ z \end{pmatrix} e^{-\frac{(x^2+y^2+z^2)}{2}}$). One-third of the nucleons in the state Ψ_1 (those for which $\Psi_1 \sim x e^{-\frac{(x^2+y^2+z^2)}{2}}$) are governed by b_1 . Thus effectively $8/3$ protons and $10/3$ neutrons of the lithium nucleus are characterized by b_0 , while $1/3$ protons and $2/3$ neutrons have the probability amplitude b_1 . Hence the scattering amplitude for the nucleus as a whole becomes

$$\begin{aligned} \left(\frac{f(\theta)}{\lambda}\right)_{\pi^-, \text{Li}} &= (8/3) b_0 \frac{f_-(\theta)}{\lambda} + (10/3) b_0 \frac{f_+(\theta)}{\lambda} + 1/3 b_1 \frac{f_-(\theta)}{\lambda} \\ &+ 2/3 b_1 \frac{f_+(\theta)}{\lambda} \quad \text{for } \pi^-, \end{aligned} \quad (11)$$

and

$$\begin{aligned} \left(\frac{f(\theta)}{\lambda}\right)_{\pi^+, L1} &= (8/3) b_0 \frac{f_+(\theta)}{\lambda} + (10/3) b_0 \frac{f_-(\theta)}{\lambda} + (1/3) b_1 \frac{f_+(\theta)}{\lambda} \\ &+ (2/3) b_1 \frac{f_-(\theta)}{\lambda} \text{ for } \pi^+, \end{aligned} \quad (12)$$

where $f_+(\theta) = F_{30} + (F_{31} + 2F_{33}) \cos \theta$

$f_-(\theta) = 1/3 [(F_{30} + 2F_{10}) + (2F_{11} + 4F_{13} + F_{31} + 2F_{33}) \cos \theta]$

are interpolated from the available pion-nucleon analyses.⁶

⁶ De Hoffmann, Metropolis, Alei and Bethe, Phys. Rev. 95, 1586 (1954)

Fermi, Metropolis and Alei, Phys. Rev. 95, 1581 (1954)

Table II lists the values of some of the quantities involved in the cross-section calculation for nine scattering angles.

Certain obvious corrections should be made in applying the above scattering amplitudes to obtain values for $d\sigma/d\Omega$ in the laboratory system. One of these is a correction for the difference in solid angles in the pion-free nucleon center of mass system and the lab system. Also a phase space correction $(p^2/v)'/(p^2/v)$ due to the increase of the pion momentum and velocity in pion-nucleon center of mass system after collision (from the unprimed to the primed values) is indicated by the general theory of reaction processes.

For scattering off the energy shell, meson theory indicates that the $f_+(\theta)$ and $f_-(\theta)$ should be taken as intermediate between the values for the initial and final c.m. energies. We have not altered these amplitudes in the calculations,

however.

If a Fourier analysis is made of Ψ_0 and Ψ_1 in equations 3 and 4, the Fourier components giving largest contribution to the integrals will be those for which $c\hbar k$ of the nucleon in the nucleus center of mass system corresponds to $-a$ before collision and $+a$ after collision. For each Fourier component of initial nucleon momentum one should, in principle, determine the incident meson kinetic energy in a Lorentz frame where the nucleon is at rest and use experimental phase shifts appropriate to that energy. There would also be solid angle and phase space corrections to the scattering amplitude that would be functions of the initial nucleon momentum. We have not attempted to carry out the above extremely complicated calculations, but it is of interest to note certain qualitative features implicit in them. For 180° scattering, a corresponds to 138.7 Mev momentum, and the meson kinetic energy in the rest frame of a proton with initial momentum $-a$ is 103 Mev. If a Fourier momentum component $-1.5a$ is chosen for the nucleon before collision the corresponding meson energy in the nucleon rest frame is 120 Mev. Since $f_+(\theta)$ and $f_-(\theta)$ at 180° increase rapidly with meson kinetic energy in the nucleon at rest frame, we might expect the 180° scattering to be better represented by applying the nuclear form factor to the scattering amplitudes associated with 100 to 120 Mev meson kinetic energies. We have accordingly carried through calculations at all angles using scattering amplitudes as well as solid angle and phase space corrections appropriate to the case of the nucleons initially

at rest. Then, at 180° , we have also carried out the calculations using scattering amplitudes and solid angle and phase space corrections appropriate to initial nucleon cp towards incident meson of 75, 124, and 207 Mev, corresponding to T_π in the nucleon rest frame of 92, 102, and 120 Mev. These calculated points are indicated on Figures 4 and 5 along with the experimental points and the calculated angular distribution assuming the nucleons initially at rest. We also show, for comparison, the effect on the 180° point of a 10 percent increase in the nuclear linear scale factor and of omitting the phase space correction - both for the case of the nucleons initially at rest.

An additional effect which we have not taken into account is the increase in kinetic energy of the meson on entering the nucleus. This would also tend to require that the scattering amplitudes $f_+(\theta)$ and $f_-(\theta)$ be chosen corresponding to higher meson kinetic energies. The experimental points in Figures 1 and 2 are relatively well matched by the theoretical curves for the nucleon at rest and $T_\pi=78$ Mev. Use of $T_\pi \sim 100$ Mev for the meson in the nucleus would give much poorer average agreement. In the 110° to 180° region the experimental points increase more rapidly than the nucleon at rest curve, and an extrapolated experimental point at 180° matches the calculated points corresponding to initial nucleon cp ~ 100 Mev directed towards the incoming meson.

It is seen that the position of the calculated curve at 180° is fairly sensitive to the choice of nuclear size, and

the difference between the experimental and calculated points near 180° for various possible initial nucleon momentum choices can be altered considerably by simultaneously choosing a value of the nuclear radius for best fit. Thus, one probably should not place too much emphasis on differences of the order of a factor of 2 at large angles between the calculated and experimental curves, in view of the overall crudeness of the theory. Rather we emphasize order of magnitude fitting of the overall features of the experimental curve.

The dip in the region of 70° is sharper in the theoretical predictions than in the experimental cross sections. Several incoherent processes, not included in the coherent addition of equations 11 and 12, may have contributed:

- a. In this region of low cross sections, multiple scatterings within the nucleus may become relatively more important, thus raising the angular distribution curve.
- b. Elastic (incoherent) spin flip scattering is possible for the proton in the p state, assuming a shell model of the nucleus. Spin flip scattering, with a $\sin \theta$ dependence, can occur at 90° , but will not be important in the backward direction.
- c. A low flying 480 Kev level with spin $1/2$ exists in lithium. Since the ground state spin is $3/2$, spin flip scattering could

give rise to an excitation of the nucleus slight enough to be included in the elastic scattering measurement.

- d. The motion of nucleons within the nucleus will produce some smearing in angle for scattering measured in the lab system, and hence degrade the sharpness of angular features.
- e. The resolution of the experiment at 70° is $\pm 4^\circ$.

Although all of the above are possible contributing factors (e) alone is sufficient to account for a large part of the difference between the experimental and theoretical curves in the region of the dip.

As mentioned earlier, one obvious feature of the experimental curves not contained in the theoretical curves is the interference between coulomb and nuclear scattering at the smallest angles. This was also seen for aluminum.⁵ It is constructive for π^- and destructive for π^+ .

The relatively good match of experimental and predicted cross sections, as well as the considerations above, show that a fairly simple single scattering model, based upon the elementary interactions of pions and nucleons, can account for the general form of the angular distribution from a light nucleus.

LIST OF TABLES

TABLE

- 1 Experimental cross sections and angular resolutions for scattering of $78 \pi^{\pm}$ from Li.

- 2 A partial listing of the factors involved in calculating 'corrected' pion-nuclear cross sections from pion-nucleon scattering amplitudes.

LIST OF FIGURES

FIGURE

- 1 Arrangement of experimental equipment.
- 2 Range curve for 80 Mev π^- .
- 3 Angular spread about the forward direction for 78 Mev π^- leaving the lithium target.
- 4 Angular distribution of 78 Mev π^- scattering by Li. The curve is the predicted angular distribution neglecting coulomb interaction and for the case described in the text as 'nucleon originally at rest'. Points a, b, c, d, e are also theoretical values, mainly at 180° , using modified assumptions. Point a omits the phase space correction. Points b are for a 10 percent larger nuclear size. Points c, d, e correspond to cases where the initial nucleon momentum is directed towards the oncoming meson with values of $(cp, cp/a, T$ of the nucleon and T_π in the nuclear rest frame) equal to (207 Mev, 1.49, 22.5 Mev, 120 Mev) for point c, (124 Mev, 0.90, 8.19 Mev, 102 Mev) for point d, (74.8 Mev, 0.54, 2.97 Mev, 92 Mev) for point e.
- 5 Similar results for 78 Mev π^+ scattering by Li. (The caption for Figure 4 applies here except for the meson charge.)

TABLE I

Experimental Cross Sections and Angular Resolutions for
Scattering 78 Mev τ^\pm from Li

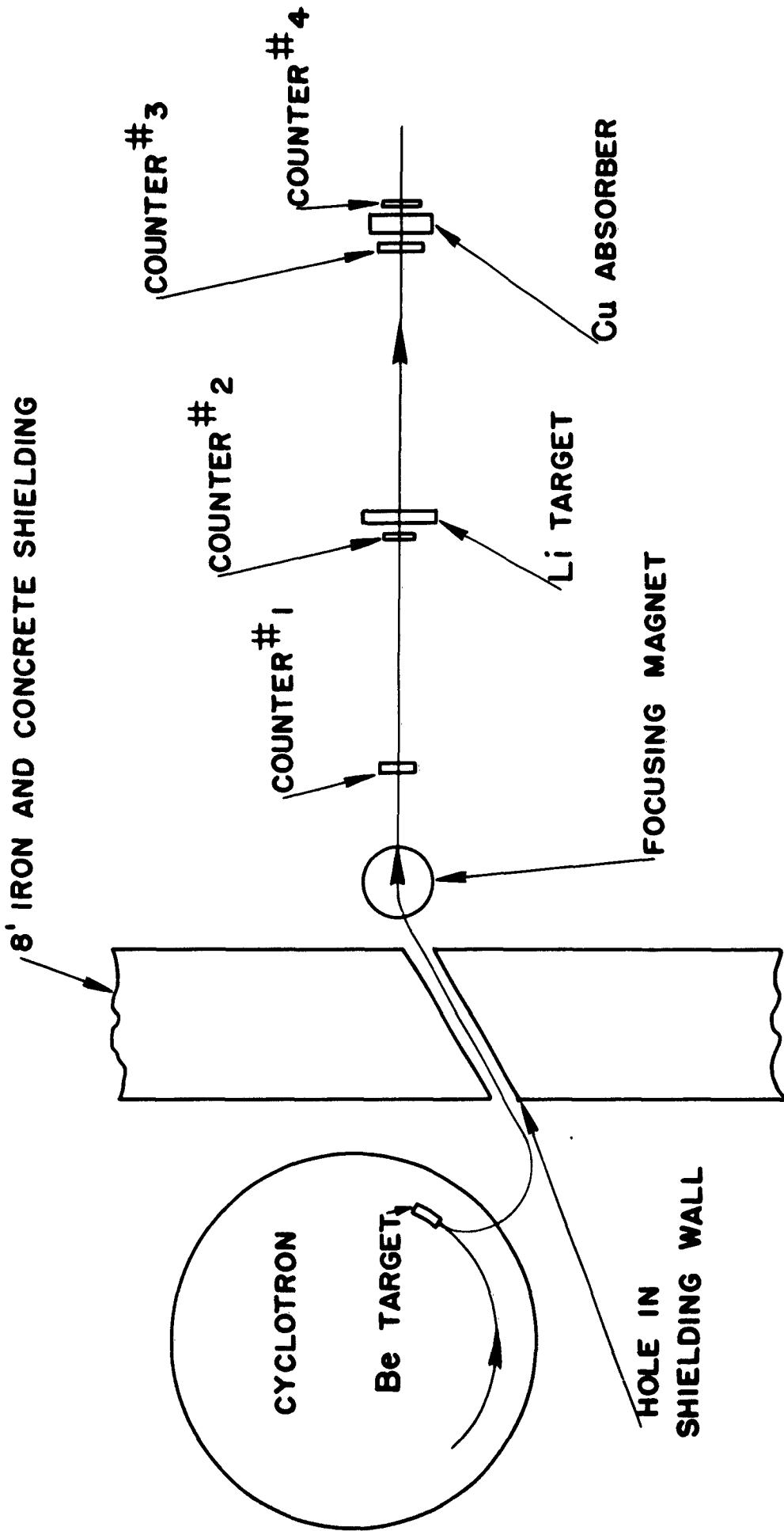
<u>78 Mev τ^-</u>			<u>78 Mev τ^+</u>		
<u>θ_{lab}</u>	<u>$(\frac{d\sigma}{d\Omega})_{mb}$</u>	<u>Angular Resolution</u>	<u>θ_{lab}</u>	<u>$(\frac{d\sigma}{d\Omega})_{mb}$</u>	<u>Angular Resolution</u>
15	233 ± 19	± 2.0°	15-1/8	124 ± 13	± 2.0°
20	84 ± 8	± 2.0°	17-3/4	53.0 ± 7.9	± 1.9°
25	61 ± 7	± 2.0°	20-5/16	30.6 ± 4.6	± 2.0°
27-1/2	49 ± 9	± 2.1°	25-1/8	32.4 ± 4.5	± 2.2°
30	44 ± 4	± 2.1°	30-5/16	28.1 ± 4.4	± 2.7°
35	30 ± 3	± 2.2°	45-3/8	12.0 ± 1.5	± 3.0°
40	22 ± 2	± 2.5°	53-7/8	5.1 ± 1.1	± 4.3°
45	18 ± 2	± 2.6°	75-1/4	1.15 ± 0.58	± 4.0°
50	10 ± 2	± 3.1°	120-1/2	4.6 ± 0.7	± 5.0°
58-3/16	4.5 ± 0.9	± 3.8°	160-5/16	6.8 ± 1.1	± 4.2°
75	2.3 ± 0.5	± 3.8°			
88-3/4	3.7 ± 0.6	± 4.8°			
90-1/16	4.0 ± 0.5	± 4.7°			
108-3/4	7.2 ± 0.9	± 4.0°			
139-5/16	11 ± 1	± 4.1°			
159	14 ± 1	± 4.1°			
170-1/4	12 ± 6	± 3.1°			

TABLE II

A Partial Listing of the Factors Involved in Calculating 'Corrected'
Pion-Nuclear Cross Sections from Pion-Nucleon
Scattering Amplitudes

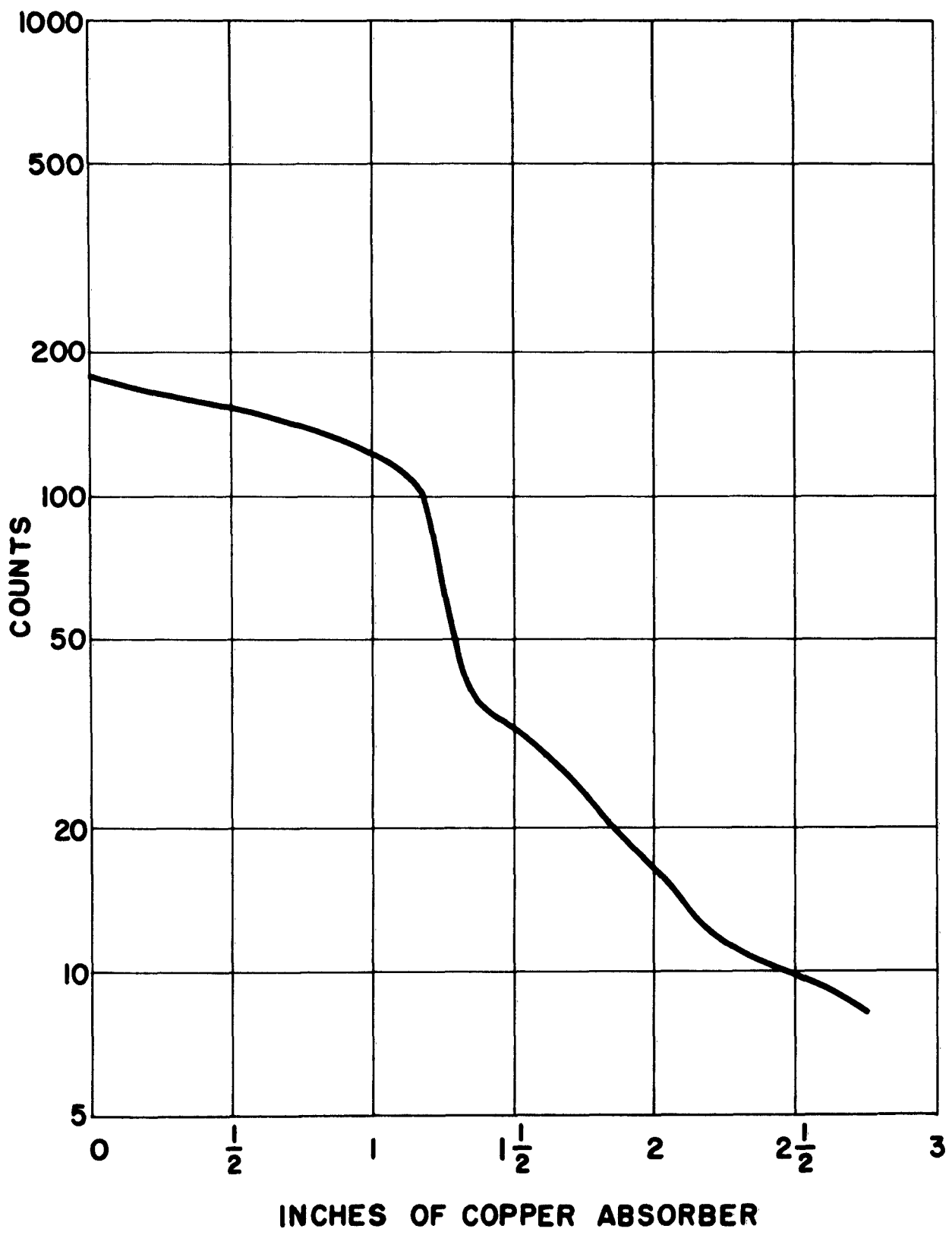
θ_{lab}	θ_{cm}^*	$\frac{\sin\theta_{cm}^* d\theta_{cm}^*}{\sin\theta_{lab} d\theta_{lab}}$	$(cp_{\pi})^2 \text{ cm}^2 B_{\pi^0 \text{ cm}}^*$	$\frac{(cp_{\pi^0})^2 B_{\pi \text{ cm}}^*}{(cp_{\pi^0})^2 \text{ cm}^2}$	$2a$	e^{-a^2}	$(1-2a^2)e^{-a^2}$	$ f(\theta) _{\pi^-}^2$	$ f(\theta) _{\pi^+}^2$
20	24°16'	1.445	1.019	.332	.988	.933	74.1 mb	64.6 mb	
40	47°48'	1.334	1.076	.655	.898	.706	27.1	25.7	
60	70°6'	1.187	1.162	.957	.795	.431	2.98	3.77	
80	91°0'	1.039	1.268	1.230	.685	.167	1.98	.231	
100	110°33'	.9105	1.381	1.467	.584	-.0439	7.42	4.53	
120	128°57'	.8107	1.488	1.658	.503	-.188	10.9	7.60	
140	146°27'	.7409	1.575	1.799	.445	-.275	11.7	8.64	
160	163°23'	.7001	1.632	1.885	.411	-.320	11.4	8.71	
180	180°	.6869	1.652	1.914	.400	-.333	11.2	8.65	

* cm refers to pion-nucleon at rest c.m. system.



EXPERIMENTAL ARRANGEMENT

RANGE CURVE 80 MEV π^-



BEAM SPREAD FROM Li TARGET: 78 MEV Π^-

